Composites Part B 94 (2016) 95–101

Contents lists available at ScienceDirect

Composites Part B

journal homepage: www.elsevier.com/locate/compositesb

Failure of CFRP-to-steel double strap joint bonded using carbon nanotubes modified epoxy adhesive at moderately elevated temperatures

Asghar H. Korayem [a, b], Shu Jian Chen [a], Qian Hui Zhang [a], Chen Yang Li [a], Xiao Ling Zhao [a], Wen Hui Duan [a, *]

[a] Department of Civil Engineering, Monash University, Melbourne, VIC 3800, Australia
[b] Department of Civil Engineering, Iran University of Science and Technology, Tehran, Iran

ARTICLE INFO

Article history:
Received 21 September 2015
Received in revised form
31 January 2016
Accepted 13 March 2016
Available online 19 March 2016

Keywords:
A. Carbon fibre
A. Particle-reinforcement
B. Interface/interphase
D. Mechanical testing

ABSTRACT

The bond characteristics of double strap joints between carbon fibre reinforced polymer (CFRP) laminates and steel with carbon nanotubes (CNTs) modified epoxy, under moderately elevated temperature (23–70 °C) were studied. The effect of CNTs on the failure modes, bond interface, and bond strength were presented. Results show that increasing test temperature causes transition of failure from epoxy-CFRP interface to steel–epoxy interface and to cohesive layer in the joints with neat epoxy. The cohesive failure could be avoided in the joints with CNT-epoxy. The observations from scanning electron microscopy revealed that CNTs bridge the cracks in epoxy matrix indicating a reinforcing effect. Moreover, CNT-epoxy can provide a significant increase (about two fold) of bond strengths at moderately elevated temperatures when compared with neat epoxy. It demonstrated that the incorporation of CNTs into the bond adhesive could allow better exploiting the potential of CFRP system in strengthening of steel structures at moderately elevated temperature.

1. Introduction

Fibre reinforced polymers (FRP) have been proved to be an excellent candidate for strengthening and rehabilitation of structures [1,2]. Their light weight, high strength, corrosion resistance and tailor-ability make them an ideal alternative for application with vast range of structures such as steel structures [3,4], concrete structures [5–8], masonry structures [9–11] and wooden structures [12]. Carbon FRP (CFRP) is commonly used for the strengthening of steel structures due to its comparable modulus with that of steel [2]. Despite the evident advantages of CFRP reinforcing technique over other conventional strengthening methods, the limited research undertaken to date shows that the exposure of CFRP-to-steel joints to moderately elevated temperature will lead to a significant reduction in the bond strength thus limiting its ability to transfer loads in the CFRP strengthening system [13–16]. The performances of CFRP-to-steel joints at moderately elevated temperatures are mainly related to two aspects: (a) the mechanical properties of CFRP and (b) the adhesion between CFRP and the steel substrate [17].

CFRP modulus is a key parameter on the failure mode of the joints at moderately elevated temperatures. Based on the definition given by Zhao and Zhang [18], the failure mode of CFRP-to-steel joints changes from CFRP delamination at room temperature to cohesive failure at 40 °C when the CFRP sheet with the modules of 240 GPa is used [13]. For the CFRP sheet with the modules of 640 GPa, CFRP rupture occurs at both room temperature and moderately elevated temperature [14]. The failure mode and bond strength of CFRP-to-steel joint under moderately elevated temperature is also dependent on the properties of the epoxy adhesive such as glass transition temperature (T_g). By using Araldite 420, MBrace Saturant and Sikadur 30 with T_g of about 42, 55 and 62 °C, respectively, in double strap joints, Ahmed et al. [15] concluded that the cohesive layer failure predominates when the test temperature is higher than the adhesive T_g. In addition, only 32% and 38% of the initial strength of the CFRP-to-steel double strap joints with MBrace Saturant and Araldite 420, respectively, remained when the joints were subjected to temperatures of 60 °C.

* Corresponding author.
E-mail address: wenhui.duan@monash.edu (W.H. Duan).

http://dx.doi.org/10.1016/j.compositesb.2016.03.042
1359-8368/

In order to increase the T_g of epoxy, different nanofillers such as, nanosilica [19], and carbon nanotubes (CNTs) [20–22] have been added to neat epoxy. Kinloch et al. [19], using concentration of about 8% by mass of nanosilica particles, reported an increase in the T_g by about 5 °C, from 70 °C to 75 °C. Gojny and Schulte [20] observed a shift on T_g from 64 °C for the neat resin, to about 80 °C for samples containing 0.75 wt.% CNTs. They concluded that functionalization of CNTs has positive effect on improving the T_g of epoxy. Recently, Asghar et al. [23] showed that 3 wt.% CNTs incorporation into neat epoxy enhances Young's modulus by 20%, tensile strength by 30%, flexural strength by 15%, and T_g by 34% of Araldite 2011 epoxy matrix.

This paper reports an experimental investigation to study the effect of CNT-epoxy on the bond behaviours of double strap joints at moderately elevated temperature. The CNT-epoxy was fabricated following the protocol developed and stated by authors elsewhere [23] and were used to fabricate the double strap joints in the current study. The failure modes of the joints were investigate via visual observation and scanning electron microscopy (SEM). The effect of CNT incorporation on the failure modes and bond strength was examined. It is discovered that the CNT in epoxy significantly improved the performance of the CRFP bonding at elevated temperature. In addition, by microscopic examination and analysis, this research provides new insight on the failure mechanism of double strap joints at moderately elevated temperature. The findings in this study contribute to a more reliable design and application of CFRP laminates in the strengthening and rehabilitation of steel infrastructures across a wider range of climates.

2. Experimental programme

2.1. Fabrication and testing of CNT-epoxy composites

The detailed procedure for the fabrication and testing of CNT-epoxy composites was reported elsewhere [23] and only the key steps are summarized here. Epoxy adhesive, CNTs, CFRP laminates and steel plates were used to fabricate CNT-epoxy composites, as well as the double strap joint specimens. The epoxy resin with commercial name of Araldite 2011, supplied by Huntsman Company (Australia), was used in this research. CNTs were multi-walled carbon nanotubes with 9.5 nm average diameter and 1.5 μm average lengths supplied by Nanocyl Company with commercial name of EpoCyl NC R128-02 Bisphenol-A master batch. CFRP laminates were normal modulus of unidirectional MBrace Laminate grade 210/3300, manufactured by BASF, with a thickness of 1.4 mm, a width of 50 mm and 70% fibre content. It has nominal elastic modulus of 210 GPa and nominal tensile strength of 3300 MPa, based on the manufacturer's specifications [24]. Steel plates were hot rolled structural steel HA300 with a thickness of 10 mm and with the same width of 50 mm as the CFRP laminates. They have a nominal yield stress of 300 MPa. The material properties and dimensions of steel plates were selected in such a way so as to avoid steel yielding during the tension loading process.

To fabricate CNT-epoxy composites, 3 wt.% CNTs and 46.11 g resin (part A) were mixed with high shear mixing homogenizer (FlackTek DAC 150.1 FVZ-K) and ultrasonication treatment, followed by degassing in a vacuum oven (ProSciTech EVAC12D). The blend was then added to 36.89 g hardener (part B) and stirred for 5 min with high shear mixer homogenizer at 300 rpm and the mixture subsequently cast into a Teflon mould. The curing cycle took 48 h at room temperature, followed by 4 h at 120 °C for the post cure. Neat epoxy was also prepared as a reference to compare with CNT-epoxy.

Dynamic mechanical thermal analysis (DMTA) was conducted using a Perkin Elmer DMA 8000 following the ASTM D4065-01 standard procedure. Rectangular specimens were used with the length of 50 mm, width of 13 mm, and thickness of 3 mm. The tests carried out under three-point-bending mode at a fixed frequency of 1 Hz and with a temperature increment of 2 °C/min. The temperature was varied from room temperature to 140 °C and T_g was taken from the peak value in the loss modulus curve.

2.2. Fabrication and testing of double strap joint samples

The effect of CNT-epoxy adhesive on the behaviour of CFRP-to-steel interface under static load at moderately elevated temperature from room temperature (23 °C) to 70 °C was examined using CFRP-to-steel double strap joints.

A schematic view of the double strap joints is shown in Fig. 1. The joints were prepared from two steel plates connected together by CFRP laminates using epoxy adhesive. CFRP laminates were chose as 270 mm ($L_1 + L_2$) where $L_1 = 120$ mm and $L_2 = 170$ mm to avoid the uncertainty of the location of debonding failure. Steel plates had a dimension of 200 × 50 × 10 mm (length × width × thickness).

Fig. 2 shows that the as-received CFRP laminates is covered by a textured surface made from a woven mesh which aids in improving the bonding with the adhesive [2]. The steel plate has a rough surface containing crevices and pores after the sandblasting which has a similar morphology presented by Teng et al. [25], and both aspects encouraged mechanical adhesion and a greater actual adhesive contact area. Epoxy adhesives in a liquid form may be able to fill in the crevices and pores on the steel surface, and provide an effective load transfer from the steel plate to the epoxy layer [26].

Both CNT-epoxy and neat epoxy were applied to investigate the effect of CNTs on the bond interface for the temperature effect as summarized in Table 2. The thickness of the adhesive was controlled as 0.4 mm for all the specimens. The specimens were cured for 48 h at room temperature and post cured for 4 h at 120 °C. Specimen designations, which start with 'P' indicate the neat epoxy adhesive and those with 'C' stand for CNT-epoxy adhesive. The number that follows the letter is the test temperature.

The specimens were tested in an environmental chamber at 23 °C, 40 °C, 50 °C, 60 °C, and 70 °C. The temperature of the test specimens was controlled using three thermocouples located in the centre of sample adjacent to CFRP laminates, adhesive layer and steel plate, respectively. To confirm that the temperature was consistent across the specimen, tensile testing did not commence until temperature differences between all three thermocouples were less than 2%.

Specimens were tested in tension based on ASTM D3528 standard procedure. The loading rate was set as 0.5 mm/min in an attempt to simulate the static loading condition. At least three samples were tested for each temperature, and the average load with standard deviation was reported. In order to measure the displacement of the joints, two linear variable differential transformers (LVDT) were used. All test data, including the loads and displacements, were recorded simultaneously by a data logger (DataTaker DT 515). To reveal the failure mechanisms of the joints, samples from the failed surfaces were cut and sputter-coated with around 1 nm thick Gold–Palladium coating materials. The samples were examined using a JEOL 7001F FEG SEM at 5 kV acceleration voltages.

3. Results and discussion

3.1. Thermo-mechanical properties of CNT-epoxy adhesives

Fig. 3 shows storage modulus and loss modulus as a function of temperature. The addition of 3 wt.% CNTs to the epoxy causes a

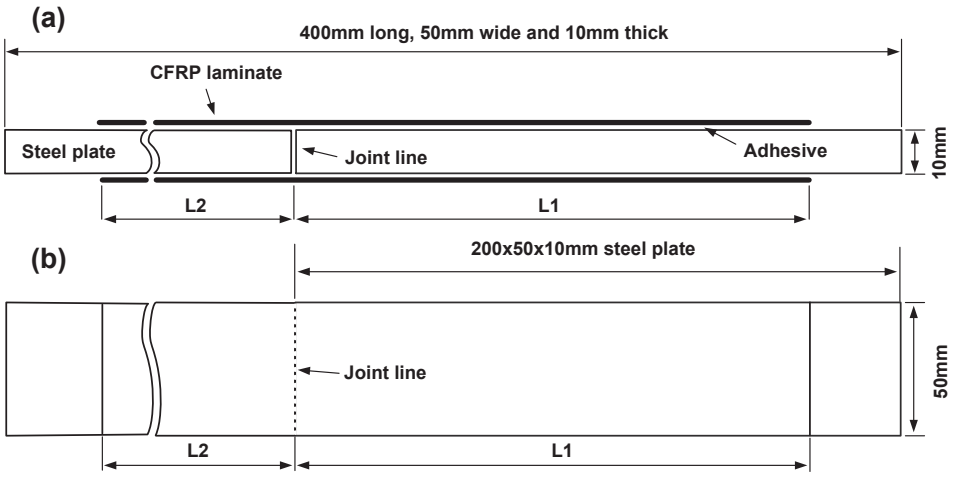

Fig. 1. A schematic view of the specimen (a) side view and (b) top view.

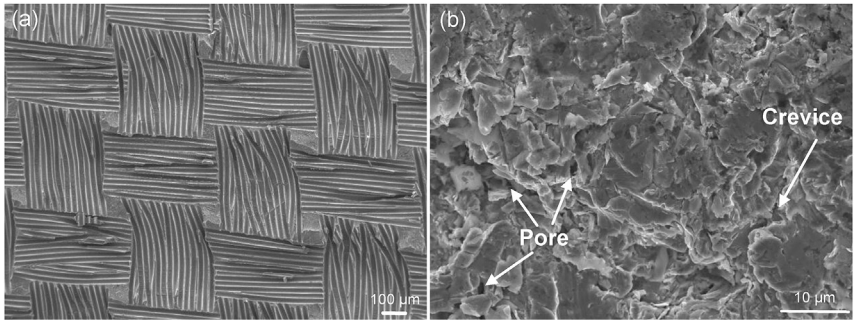

Fig. 2. SEM images of (a) surface of as-received CFRP laminates covered by a woven mesh and (b) the rough surface of steel plate after sandblasting [27].

Table 1
Tensile properties and T_g of the neat epoxy and CNT-epoxy adhesive.

Epoxy	Tensile modulus (GPa)	Tensile strength (MPa)	Ultimate strain (%)	T_g (°C)
Neat epoxy	1985 (±33[a])	40.0 (±0.4)	12.7 (±2.0)	46.2 (±1.1)[b]
CNT-epoxy	2391 (±14)	52.4 (±0.3)	7.5 (±2.4)	59.7 (±1.4)

[a] Standard deviation.
[b] 45 °C provided from suppliers.

Table 2
Specimens details and their failure mode.

Specimen	Test temperature (°C)	Adhesive	t_a (mm)	P_u (kN)	$(P_u/P_{u\text{-}23}) \times 100\%$
P23	23	Neat epoxy	0.35	142.8 (±0.3[a])	100.0
P40	40	Neat epoxy	0.39	47.6 (±4.0)	33.3
P50	50	Neat epoxy	0.39	26.5 (±0.5)	18.6
P60	60	Neat epoxy	0.35	18.7 (±0.6)	13.1
P70	70	Neat epoxy	0.36	13.1 (±4.2)	9.2
C23	23	CNT-epoxy	0.35	133.1 (±4.6)	100.0
C40	40	CNT-epoxy	0.32	92.5 (±0.4)	69.5
C50	50	CNT-epoxy	0.32	49.5 (±1.8)	37.2
C60	60	CNT-epoxy	0.32	34.9 (±4.6)	26.2
C70	70	CNT-epoxy	0.34	25.4 (±2.8)	19.1

t_a: adhesive thickness (0.4 mm for the intended thickness). The average adhesive thickness was calculated using the method described in Wu et al. [33].
$P_{u\text{-}23}$: the bond strength at the room temperature 23 °C.
[a] Standard deviation.

slight raise onto storage modulus on the rubbery regions. However, a strong increase was observed in the storage modulus in glassy regions and in the vicinity of the glass transition temperature T_g. The neat epoxy has the T_g of 46.2 °C, which is consistent with the 45 °C provided by supplier, whilst the CNT-epoxy possesses a T_g of 59.7 °C which shows an improvement of about 30%. It is thus able to improve the elastic properties of the epoxy system at moderately elevated temperatures. The tensile properties reported in Ref. [23]

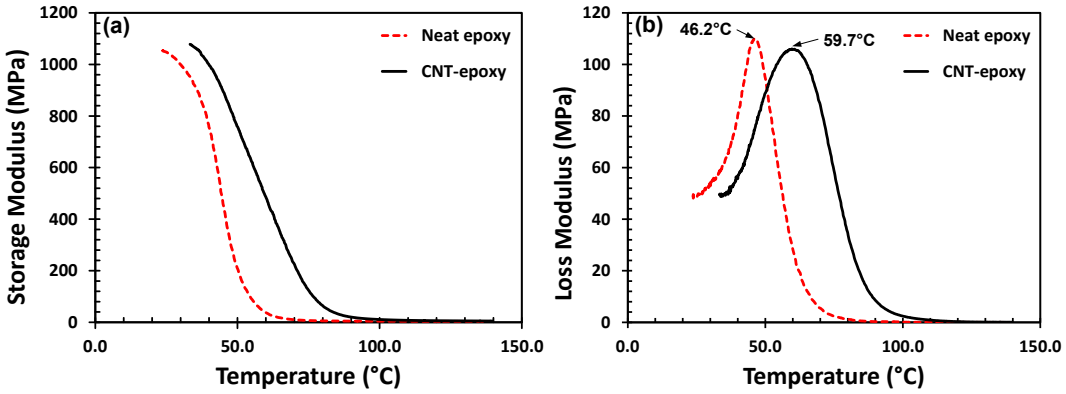

Fig. 3. Thermo-mechanical properties: (a) storage modulus and (b) loss modulus of neat epoxy and 3 wt.% CNT-epoxy composites [23].

and thermo-mechanical properties of CNT-epoxy and neat epoxy summarized in Table 1. The incorporation of CNTs into neat epoxy leads to an increase about 20% in Young's modules and 30% in tensile strength, respectively, although the maximum elongation is reduced about 41%.

3.2. Failure modes from the view of macro-level

The typical failure modes at different temperature are shown in Fig. 4. For the bond with neat epoxy, i.e. P23, P40, P50, P60, and P70, the failure modes are the combination of steel–epoxy interface, epoxy-CFRP interface and cohesive layer [2,18]. When the temperature is relatively low, i.e. P23 and P40, more epoxy-CFRP interface failure occurs whereas cohesive layer failure predominates with increasing temperature, i.e. P70. The steel–epoxy interface failure can be observed at the medium range of temperature, i.e. P50 and P60. It is clear that the failure modes of the specimens transit from epoxy-CFRP interface to steel–epoxy interface and cohesive layer with increasing temperature.

This transition could be explained as follows. At the room temperature, the weak bonding between woven mesh and CFRP fibres are the main cause for the premature failure of the double strap joints, as demonstrated in our previous work [27]. When the temperature increases to the medium range, say about 40 °C, the thermal stress in the steel–epoxy interface begins to play a role. Hart-Smith [28] calculated the shear stress of the double strap joints due to the mismatch of the coefficient of thermal expansion (CTE) between two different adherents. The maximum thermal shear stress along the bond line due to the elevated temperature has been given by Ref. [29].

$$\tau_{max} = \frac{G}{\beta\eta}(\alpha_p - \alpha_s)(T_c - T_t) \quad (1)$$

$$\beta^2 = \frac{G}{\eta}\left(\frac{2}{E_s t_s} + \frac{1}{E_p t_p}\right) \quad (2)$$

where τ is the thermal shear stress at the steel–epoxy interface, (E_p, E_s), (t_p, t_s) and (α_p, α_s) the elastic modules, thicknesses, and CTE of CFRP laminates and steel, respectively, T_c and T_t curing temperature and test temperatures, respectively, G shear modulus of epoxy, and η the thickness of epoxy adhesive layer. Assuming that the CTE of steel and CFRP laminates are 11×10^{-6} and 0.6×10^{-6}, respectively and the curing temperature 23 °C, the maximum thermal shear stress at steel–epoxy interface at test temperature 40 °C can be calculated as −3.7 MPa based on Eq. (1). The negative thermal stress indicates that the bond strength to resist the applied load is

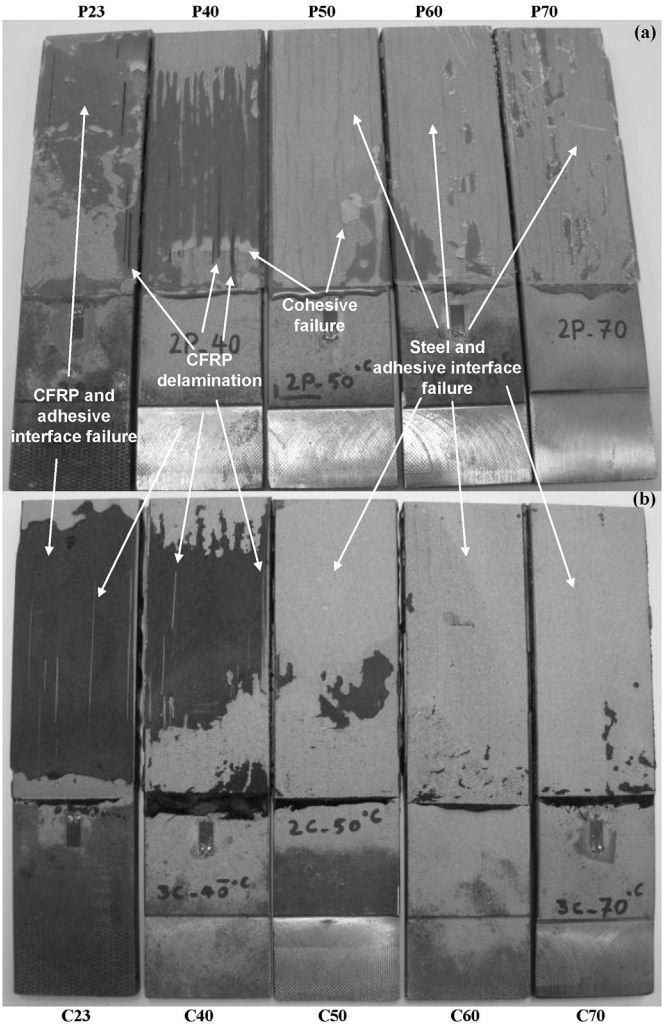

Fig. 4. Failure modes of joints bonded with (a) neat epoxy and (b) CNT-epoxy adhesive at different temperatures.

effectively reduced. Therefore, at temperatures of the medium range (40–60 °C), the thermal stress due to the mismatch CTE between steel and epoxy increases the stress level between the steel–epoxy interface and cause its failure prior to the epoxy-CFRP interface failure.

When the temperature continues above 60 °C (T_g for neat epoxy is 46.2 °C), the thermal stress between steel and epoxy further increases. In addition, the neat epoxy starts to lose strength, and thus the combination of the steel–epoxy interface failure and the cohesive layer failure can be observed in the specimen P70. For the specimens with CNT-epoxy, there are only two failure modes within the temperate range of 23–70 °C, i.e. epoxy-CFRP interface at the temperature below 40 °C and steel–epoxy interface at the temperature above 40 °C. Again the epoxy-CFRP interface failure is due to the weak bonding between woven mesh and CFRP fibres. At the moderately elevated temperatures, the thermal stress between steel and epoxy causes the steel–epoxy interface failure. The cohesive layer failure no longer happens due to the significant improvement of T_g, from 46.2 °C for neat epoxy to 59.7 °C for CNT-epoxy.

3.3. Bond interface from microscopic observations

The failure modes discussed in Section 3.2 are defined from the macroscopic or structural perspective. Further analysis of the SEM micrographs for the steel–epoxy interface, epoxy-CFRP interface and cohesive layers are discussed to promote a better comprehension of the mechanism responsible for the different failure modes. SEM images on the failure surfaces corresponding to different failure modes are shown in Fig. 5. The locations the SEM images were taken within the double strap joint are given by Fig. 5(a). Left and middle columns of the SEM images represent the joints with neat epoxy and CNT-epoxy joint, respectively. The closer views of the SEM images in middle column are shown in the right column.

Fig. 5(b1) shows the failure surface of epoxy layer from the epoxy-CFRP interface. It is clear that the failure modes are the combination of epoxy-CFRP interface due to the weak bonding between the woven mesh and CFRP fibres, as well as the cohesive failure in epoxy layer. The cracks propagate into the epoxy layer attached with the woven mesh. The combination of epoxy-CFRP interface and cohesive failure is also observed for CNT-epoxy as shown in Fig. 5(b2). However, the CNTs indeed reinforce the epoxy layer as evidenced in Fig. 5(b3). The CNTs are uniformly distributed within the epoxy matrix indicating the good dispersion. In addition, the CNTs are pulled out from the epoxy and are perpendicular to the fracture surface, contributing to the energy-absorbing bridging effect [30,31].

The failure surface of epoxy layer is shown in Fig. 5(c1) from the steel–epoxy interface. As the same in Fig. 5(b1) and (b2), the cracks propagate into the epoxy layer. In addition, the cracks form a chain [32] which will consume more energy during the failure process in both neat epoxy and CNT-epoxy. Again, the reinforcing effect of CNTs is clearly evidenced in Fig. 5(c3).

Fig. 5(d1) and (d2) show the failure surface of steel surface from the steel–epoxy interface. The failure surfaces are rather flat with epoxy filling the crevices and pores on the steel surface well. The epoxy in these crevices and pores failed in the shear due to the elevated temperature instead of detachment of epoxy from steel surface. In Fig. 5(d3), the CNTs can be observed in a good dispersion and reinforcing effect.

Fig. 5(e1) and (e2) show the failure of CFRP laminates from the epoxy-CFRP interface. In both images there are the traces of woven mesh on the residual epoxy indicating a weak bonding between woven mesh with CFRP fibres. More importantly, the delamination of CFRP fibres can be observed. This can be attributed to the relatively low T_g of epoxy in the CFRP laminates. The delamination of CFRP fibres is more severe in the joint with CNT-epoxy, likely due to higher T_g of the CNT-epoxy layers which can transfer increased load from the steel to CFRP laminates at moderately elevated temperatures.

3.4. Load displacement relationship

The load–displacement relationship for the double strap joints bonded with neat epoxy and CNT-epoxy adhesive at moderately elevated temperatures is given in Fig. 6. In both cases, the loads increase linearly at relatively small displacement until the ultimate loads are achieved. For neat epoxy system, the slope of the curves decreases with increasing temperature and the stiffness of the joints is reduced. The reduction of the stiffness commences at 50 °C, which is closer to its T_g 46.2 °C, as shown in Fig. 3. In contrast, the reduction of the joint stiffness for CNT-epoxy starts at higher temperature, 60 °C, corresponding to its T_g.

Bond strengths (P_u) derived from the data in Fig. 6 are summarized in Table 2. At the moderately elevated temperature, the bond strengths for CNT-epoxy adhesive are significantly higher than those for neat epoxy adhesive. For example, at 50 °C and 60 °C corresponding to the T_g for neat epoxy and CNT-epoxy, respectively, the bond strengths for CNT-epoxy, 49.5 and 34.9 kN, are about 2-fold of those for neat epoxy, 26.5 and 18.7 kN, respectively. When compared with the bonds at room temperature (23 °C), the bond strengths at 70 °C are reduced to 9.2% and 19.1% for neat epoxy and CNT-epoxy, respectively.

The improved bond strengths can be attributed to the higher storage modulus and T_g of CNT-epoxy compared to those of neat epoxy as shown in Fig. 3. This makes clear that the increase in T_g from 46.2 to 59.7 °C is very important since the temperature on the surface of steel infrastructures could reach 40–60 °C in hot summer. The conventional adhesive will soften and the bond strength will be significantly reduced [13]. By using the CNT-epoxy, the reduction of the bond strength at moderately elevated temperature can be partially avoided. It should be noted that standard deviation of tested P_u (Table 2) is within a consistent level (<4.6 kN) for the 10 sets of specimens tested at different temperatures. The differences in P_u due to the temperature increment and the addition of CNTs (~10–100 kN) is much larger than the standard deviation. Therefore, experimental error presents minimum effect on the conclusion that P_u decreases with elevated temperature and increase due to CNT addition.

4. Conclusions

In this paper, the effect of temperature on the failure of CFRP-to-steel double strap joints with neat epoxy and CNT-epoxy adhesives were investigated via mechanical tests and SEM observations. It was found that within the temperate range of 23–70 °C, failure mode of the joints with neat epoxy changes from the epoxy-CFRP interface at temperatures below 40 °C, to the steel–epoxy interface at temperatures from 50 to 60 °C and to cohesive failure at temperature above 60 °C. In contrast, the joints with CNT-epoxy failed at the epoxy-CFRP interface below 40 °C and at steel–epoxy interface above 40 °C due to the improved T_g of CNT-epoxy compared with neat epoxy. Thermal stresses induced by the mismatch of CTE between steel and CFRP laminates plays a role for the steel–epoxy interface failure.

From the microscopic observations, the bridging effect of CNTs with a uniform distribution in epoxy layer was observed at the crack surface within the epoxy layer and residual epoxy on the steel surface. The delamination of CFRP fibres is more severe in CNT-epoxy layer due to the higher T_g of CNT-epoxy, by which CNT-epoxy layer can transfer more loads from steel to CFRP laminates.

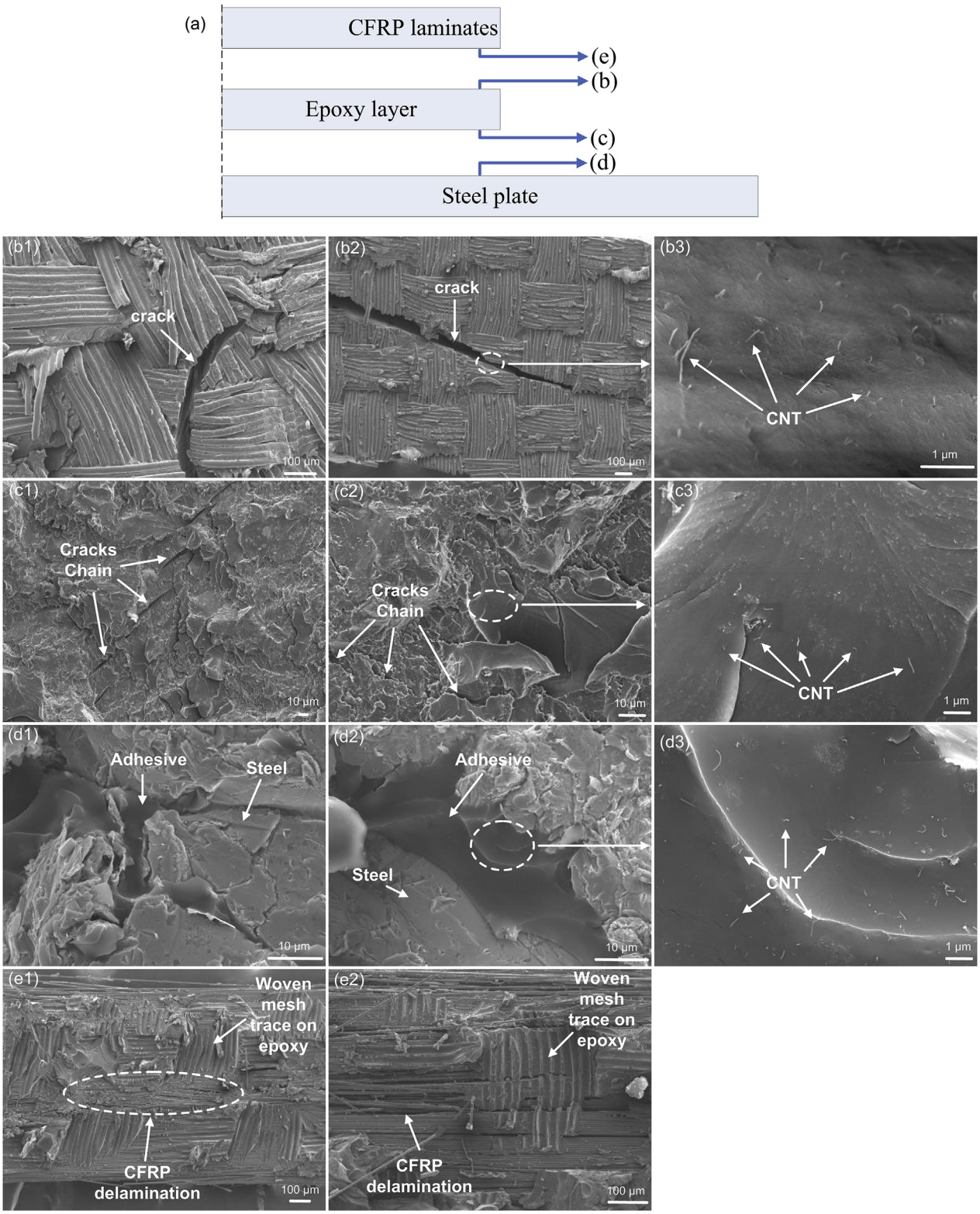

Fig. 5. (a) Locations of SEM images within CFRP-to-steel joint interfaces, and failure surface of the joints with neat epoxy (b1–e1 at the temperature of 50 °C) and CNT-epoxy (b2–e2 at the temperature of 70 °C) as well as the close view of CNT-epoxy (b3–d3).

For the joints with CNT-epoxy, the reduction of the stiffness starts at a higher temperature due to the improved T_g. CNT-epoxy can provide a significant increase (about two fold) of bond strengths at moderately elevated temperatures. This could allow increasing the maximum service temperature of steel infrastructure strengthened with CFRP systems, a key main challenge for FRP systems used in civil engineering applications.

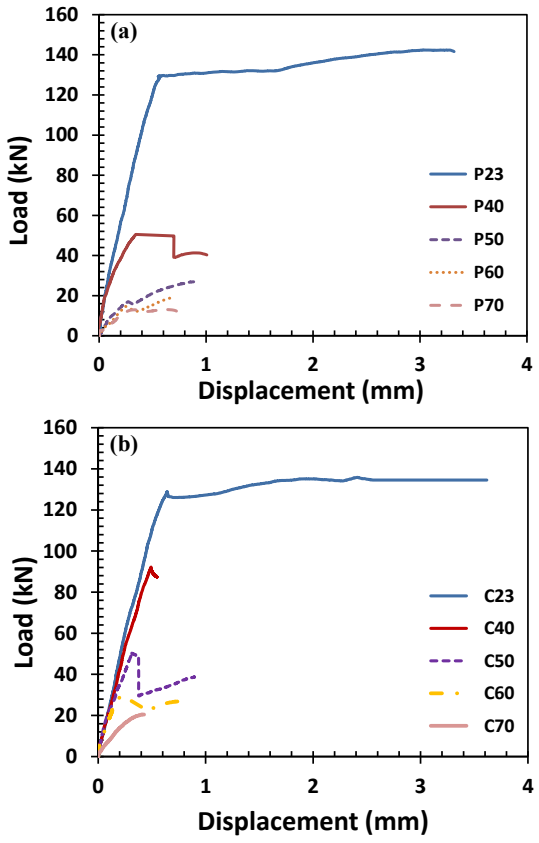

Fig. 6. Load displacement curves of joints bonded with (a) neat epoxy and (b) CNT-epoxy adhesive at different test temperatures.

Acknowledgement

Authors are grateful for the financial support of the Australian Research Council in conducting this study. AHK thanks the financial support from the Ministry of Science, Research and Technology of Iran. Authors acknowledge the use of facilities within the Monash Centre for Electron Microscopy. Authors thank Professor G. P. Simon in Department of Materials Engineering at Monash University for reading the manuscript.

References

[1] Heshmati M, Haghani R, Al-Emrani M. Environmental durability of adhesively bonded FRP/steel joints in civil engineering applications: state of the art. Compos Part B Eng 2015;81:259–75.
[2] Teng Jg, Yu T, Fernando D. Strengthening of steel structures with fiber-reinforced polymer composites. J Constr Steel Res 2012;78:131–43.
[3] Agarwal A, Foster SJ, Hamed E. Wet thermo-mechanical behavior of steel–CFRP joints – an experimental study. Compos Part B Eng 2015;83:284–96.
[4] Yu T, Fernando D, Teng Jg, Zhao XL. Experimental study on CFRP-to-steel bonded interfaces. Compos Part B Eng 2012;43(5):2279–89.
[5] Boumarafi A, Abouzied A, Masmoudi R. Harsh environments effects on the axial behaviour of circular concrete-filled fibre reinforced-polymer (FRP) tubes. Compos Part B Eng 2015;83:81–7.
[6] Tanapornraweekit G, Haritos N, Mendis P, Ngo T. Finite element simulation of FRP strengthened reinforced concrete slabs under two independent air blasts. Int J Prot Struct 2010;1(4):469–88.
[7] Rousakis TC, Saridaki ME, Mavrothalassitou SA, Hui D. Utilization of hybrid approach towards advanced database of concrete beams strengthened in shear with FRPs. Compos Part B Eng 2016;85:315–35.
[8] Yazdani N, Goucher E. Increasing durability of lightweight concrete through FRP wrap. Compos Part B Eng 2015;82:166–72.
[9] Fabbrocino F, Farina I, Berardi VP, Ferreira AJM, Fraternali F. On the thrust surface of unreinforced and FRP-/FRCM-reinforced masonry domes. Compos Part B Eng 2015;83:297–305.
[10] Faella C, Martinelli E, Camorani G, Aiello MA, Micelli F, Nigro E. Masonry columns confined by composite materials: design formulae. Compos Part B Eng 2011;42(4):705–16.
[11] Maljaee H, Ghiassi B, Lourenço PB, Oliveira DV. Moisture-induced degradation of interfacial bond in FRP-strengthened masonry. Compos Part B Eng 2016;87:47–58.
[12] Mosallam AS. Structural evaluation and design procedure for wood beams repaired and retrofitted with FRP laminates and honeycomb sandwich panels. Compos Part B Eng 2016;87:196–213.
[13] Nguyen T-C, Bai Y, Zhao XL, Al-Mahaidi R. Mechanical characterization of steel/CFRP double strap joints at elevated temperatures. Compos Struct 2011;93(6):1604–12.
[14] Liu HB, Zhao XL, Bai Y, Raman RKS, Rizkalla S, Bandyopadhyay S. Bond tests of high modulus CFRP/steel double-strap joints at elevated temperatures, in ACUN6. 2012. Melbourne, Australia.
[15] Al-Shawaf A, Al-Mahaidi R, Zhao XL. Effect of elevated temperature on bond behaviour of high modulus CFRP/steel double-strap joints. Aust J Struct Eng 2009;10(1):63–74.
[16] Habibnejad Korayem A, Liu YM, Zhao XL, Duan WH. Bond characterization of steel-CFRP with carbon nanotube modified epoxy adhesive via pull-off tests. Int J Struct Stab Dyn 2015;15(8). 1540027.
[17] Di Ludovico M, Piscitelli F, Prota A, Lavorgna M, Mensitieri G, Manfredi G. Improved mechanical properties of CFRP laminates at elevated temperatures and freeze–thaw cycling. Constr Build Mater 2012;31:273–83.
[18] Zhao XL, Zhang L. State-of-the-art review on FRP strengthened steel structures. Eng Struct 2007;29(8):1808–23.
[19] Kinloch A, Lee J, Taylor A, Sprenger S, Eger C, Egan D. Toughening structural adhesives via nano-and micro-phase inclusions. J Adhesion 2003;79(8–9):867–73.
[20] Gojny FH, Schulte K. Functionalisation effect on the thermo-mechanical behaviour of multi-wall carbon nanotube/epoxy-composites. Compos Sci Technol 2004;64(15):2303–8.
[21] Ma PC, Kim J-K, Tang BZ. Effects of silane functionalization on the properties of carbon nanotube/epoxy nanocomposites. Compos Sci Technol 2007;67(14):2965–72.
[22] Shen J, Huang W, Wu L, Hu Y, Ye M. The reinforcement role of different amino-functionalized multi-walled carbon nanotubes in epoxy nano-composites. Compos Sci Technol 2007;67(15–16):3041–50.
[23] Habibnejad Korayem A, Barati MR, Simon GP, Zhao XL, Duan WH. Reinforcing brittle and ductile epoxy matrices using carbon nanotubes masterbatch. Compos Part A Appl Sci Manuf 2014;61:126–33.
[24] BASF. BASF The Chemical Company. 2013; Available from:http://www.basf-cc.com.au/.
[25] Teng JG, Fernando D, Yu T, Zhao XL. Debonding failures in CFRP-strengthened steel structures. In: Proceedings third Asia–Pacific Conference on FRP in structures (APFIS2012); 2012 [Japan].
[26] Chawla KK. Composite materials: science and engineering. , New York: Springer; 2012.
[27] Habibnejad Korayem A, Li CY, Zhang QH, Zhao XL, Duan WH. Effect of carbon nanotube modified epoxy adhesive on CFRP-to-steel interface. Compos Part B Eng 2015;79:95–104.
[28] Hart-Smith LJ. Adhesive-bonded double lap joints. Long beach California, USA: Douglas Aircraft Company; 1973.
[29] Chen W, Nelson C. Thermal stress in bonded joints. IBM J Res Dev 1979;23(2):179–88.
[30] Qian D, Dickey EC, Andrews R, Rantell T. Load transfer and deformation mechanisms in carbon nanotube-polystyrene composites. Appl Phys Lett 2000;76(20):2868–70.
[31] Ajayan PM, Schadler LS, Giannaris C, Rubio A. Single-walled carbon nanotube–polymer composites: strength and weakness. Adv Mater 2000;12(10):750–3.
[32] Wetzel B, Rosso P, Haupert F, Friedrich K. Epoxy nanocomposites – fracture and toughening mechanisms. Eng Fract Mech 2006;73(16):2375–98.
[33] Wu C, Zhao XL, Duan WH, Al-Mahaidi R. Bond characteristics between ultra high modulus CFRP laminates and steel. Thin-Walled Struct 2012;51:147–57.